

37. Vegetation–Climate Feedbacks in Transient Simulations Over the Last Interglacial (128 000–113 000 yr BP)

M. Gröger¹, E. Maier-Reimer¹, U. Mikolajewicz¹, G. Schurgers¹, M. Vizcaino¹ and A. Winguth²

¹Max-Planck-Institut für Meteorologie, Bundesstraße 53, D-20146 Hamburg

²Center for Climatic Research, Department of Atmospheric and Oceanic Sciences, 1225 W, Dayton St Madison, WI 53706, USA

ABSTRACT

The presently developed MPI/UW 3D – Earth system model for long-term integrations is applied to simulate the climate of the last interglacial. The model consists of an atmospheric and oceanic general circulation model, a dynamical terrestrial vegetation model and a marine carbon cycle model.

The model was forced with time-varying insolation from 129 000 to 113 000 years before present (yr BP), revealing substantial feedbacks from the land biosphere on climate. These turned out to be important both for the simulated temperature in high northern latitudes and for the precipitation in the northern hemisphere monsoon belt. During the Eemian warm period, the simulated boreal forest extends in many places till the Arctic Ocean, and during the following cold period the transition between tundra and taiga migrated further south. Furthermore, associated albedo changes strongly amplify the simulated temperature changes.

The intensified summer insolation during the Eemian leads to a higher precipitation over continents in the northern hemisphere. The strongest response is seen in the tropics and the African-Asian monsoon belt due to increased land–sea temperature contrasts. Vegetation is established in the Western Sahara desert. Compared to simulations with land vegetation prescribed at present-day pattern, the amount of precipitation in the Sahara is more than twice as large. The simulations show strong impacts on the

time-transient climate response by triggering nonlinear delays and accelerations seen in various atmospheric and oceanic temperature time series.

The simulated storage of carbon in the terrestrial biosphere is relatively large. The carbon storage in land vegetation is increased by more than 10% during the Eemian compared to the following cold period. The associated changes in storage in soil and litter account for more than 100 GtC.

37.1 INTRODUCTION

The last interglacial period provides a complex pattern of climatic changes that culminated in the growth of large-scale continental ice sheets over North America and Scandinavia, motivating comprehensive and multidisciplinary modelling strategies. During this period, the northern hemisphere summer insolation declined from values larger than today in the early Eemian to a minimum at around 115 000 yr BP (see Chapter 2, Berger *et al.*, this volume). Model studies covering this period have applied either less comprehensive models (typically coupled ocean–atmosphere or atmosphere-only models) or Earth system models of intermediate complexity that are higher parameterized. During the Eemian warm period, the main features found in these studies is a strong warming north of ~30°N (Harrison *et al.*, 1995; Montoya *et al.*, 1998, 2000; Kubatzki *et al.*, 2000; Crucifix

and Loutre, 2002) and an intensified summer monsoon in the northern hemisphere (Kubatzki *et al.*, 2000; Montoya *et al.*, 2000). By contrast, cooling especially in boreal regions was simulated in studies focusing on the late Eemian when large-scale continental ice sheets started to grow (Crucifix and Loutre, 2002; Meissner and Gerdes, 2002; Yoshimori *et al.*, 2002; Meissner *et al.*, 2003).

However, the climate response to orbital forcing is further complicated by internal climate variability, nonlinear feedbacks and interactions between individual climate components that damp or amplify the response to orbital forcing. In particular, the glacial inception must have been heralded and paralleled by important feedback loops between individual climate components including changes in ocean circulation, vegetation, albedo and greenhouse gases. Recent work has already emphasized important feedbacks for the glacial inception. Albedo-temperature feedbacks north of 60°N were found to be driven by changes in snow coverage, sea-ice and vegetation (Crucifix and Loutre, 2002; Meissner *et al.*, 2003). The role of oceanic circulation changes was highlighted by Meissner and Gerdes (2002).

Another climate phenomenon highly sensitive to variations in insolation is the global monsoon system. Many studies found a strengthening of the monsoon precipitation in the northern hemisphere during periods when insolation was enhanced. This is suggested by a large number of model simulations (Claussen and Gayler, 1997; Levis *et al.*, 2004) and corroborated by palaeoclimatic reconstructions (Larrasoana *et al.*, 2003; Yuan *et al.*, 2004).

In this study, we will focus on the preconditions for glacial inception and the monsoon intensity in the northern hemisphere. Emphasis is laid on feedbacks arising from the terrestrial biosphere in time-transient and insolation-forced simulations. The terrestrial biosphere can influence climate via two major approaches. In a biophysical line

of evidence, vegetation alters the land surface, which affects the lower boundary condition for the atmosphere primarily by controlling the surface albedo and absorption of short-wave radiation. In addition to this, on a global scale, the terrestrial biosphere can act as source or sink for greenhouse gases in climate change scenarios. Although the biophysical and biochemical feedbacks operate contemporaneously in the real world, only few model studies did account for them simultaneously and in a full prognostic mode (Claussen *et al.*, 2001). This is a drawback, since the two feedbacks can have opposite impact on climate giving rise to a complex, nonlinear pattern of climate response. Hence in this study, attention is focused on feedbacks associated with terrestrial vegetation and carbon cycle by using an Earth system model in which the dynamics of these feedbacks are explicitly described.

37.2 MODEL, EXPERIMENTAL SETUP

The atmospheric component of the ESM used in this study consists of the ECHAM3 GCM with a horizontal resolution of ~5.6 degrees and 19 vertical levels (Roeckner *et al.*, 1992). The physical ocean component is an improved version of the Hamburg large-scale geostrophic ocean model (Maier-Reimer *et al.*, 1993) including a thermodynamic sea-ice model. The oceanic component run on a 64X64 E grid (Arakawa and Lamb, 1977), resulting in a horizontal resolution of approximately 4 degrees and 22 vertical levels. Continental ice sheets are prescribed at present-day pattern. The terrestrial biosphere is the Lund-Potsdam-Jena (Sitch *et al.*, 2003) dynamic global vegetation model (DGVM) running with the same horizontal resolution as used for the atmosphere. The LPJ models vegetation as 10 different plant functional types (PFT) that fractionally inhabit the grid space. The distribution of PFT is related to climatic boundary conditions for plant growth,

regeneration and plant-specific parameters that control plant competition for light and water. Carbon storage is calculated in living biomass, litter and soils. Climatic feedbacks from the terrestrial biosphere are provided to the atmosphere via monthly means of surface background albedo, vegetation cover, forest cover and roughness length.

The model used here holds an interim position between higher resolution complex AOGCMs (used primarily for relatively short-term simulations (Chapter 33 Kaspar *et al.*, Chapter 34, Widmann) and more economic models of intermediate complexity with less explicitly modelled processes (used for long-term integrations, Chapter 36 Loutre *et al.*, Chapter 38 Kageyama *et al.*, Chapter 39, Kubatzki *et al.*).

Since the typical adjustment times of individual climate components are in the same order as their characteristic timescales, this allows to integrate the highly dynamic (and computational consumptive) model components only from time to time. Therefore, in order to save computational resources, a periodically synchronous coupling scheme is applied after Voss and Sausen (1996). Accordingly, the atmospheric component is switched off after integrating for 24-month periods. In the following asynchronous periods the length of which is determined interactively (10 years on average), the fluxes from previous synchronous periods are used to drive the other model components. A nonlinear energy balance model is used to damp SST and sea-ice anomalies during the asynchronous periods. For the vegetation model LPJ, an archive consisting of input parameters of the last four synchronous periods was used in order to generate some variability. This was necessary to avoid a model drift.

The constant forcing applied in equilibrium simulations is appropriate for the study of internal climate feedbacks but neglects the specific adjustment times of different climate components. Kubatzki *et al.* (this volume) demonstrate in chapter 39 that time-slice experiments differ significantly

from transient runs simulating the glacial inception. Therefore, in this study a time-transient insolation forcing has been applied.

All experiments presented here were started from restart files derived from a $\sim 10\,000$ -year integration of the fully coupled model under present-day boundary conditions. In order to assess the biophysical impact from the terrestrial biosphere on climate, two sets of experiments were carried out. In one set, the land-surface conditions for the atmosphere and glacier mask were fixed according to present-day conditions (ECHAM3 land surface, without biophysical feedback). In the second set of experiments, the dynamic changes in vegetation simulated by the LPJ were used to update the surface boundary condition for the atmosphere (with biophysical feedback). Each set consists of a control run with present-day insolation and an Eemian run in which the model has been forced with time-varying insolation according to an orbital configuration corresponding to the period from 129 000 to 113 000 yr BP. The first thousand years are excluded from consideration, because of possible spinup effects. In the Eemian experiments, the forcing has been accelerated by a factor of eight. This tightens the carbon fluxes between the atmosphere and the sources of disturbance and thus, limits the interpretation of $p\text{CO}_2$ to the detection of long-term trends rather than permitting quantitative examinations.

In the following, a brief description of the forcing is given. In Section 3, internal climate feedbacks will be investigated by difference fields between selected time slices that represent the minimum and maximum climatic extremes. Emphasis is laid on climate feedbacks from dynamic vegetation changes. Finally, the time-transient evolution is analysed using time series from selected climate parameters.

The daily values of incoming solar radiation at the top of the atmosphere have been calculated from the obliquity, eccentricity

and the longitude of the perihelion using the algorithm of Berger and Loutre (1991) and a solar constant of 1365 W/m^2 . The results have been adapted to the 360 day-year used in the model.

The time-transient changes in the orbital parameters cause only minor changes in the yearly mean insolation. In the course of the Eemian, the insolation decreases only by about 3 W/m^2 . In the early Eemian, however, the seasonal contrast was amplified in the northern hemisphere. As a consequence, the northern hemisphere received considerably more insolation in the early part of the Eemian (Fig. 37.1a). Because of the increased

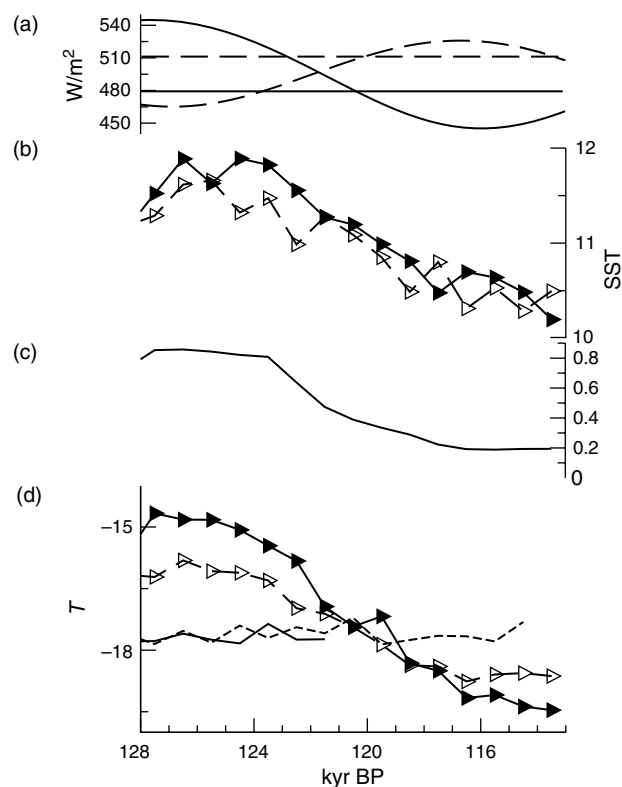


Fig. 37.1 Time series of (a) yearly maximum of daily mean insolation at 60°N and 60°S (dashed curve). Straight lines indicate present-day values. (b) North Atlantic sea-surface temperatures north of 30°N . Dashed line indicates experiment without feedback. (c) vegetation cover [fraction] averaged over 60° to 90°N . (d) Near-surface temperatures overland points north of 60°N . Dashed lines indicate the simulations without feedback. Thin lines indicate control experiments. Displayed are 1000-year averages.

obliquity, the insolation changes are more pronounced in the higher latitudes in the early parts of the Eemian. For a detailed description about the Eemian insolation pattern, we refer to Chapter 2 (Berger *et al.*, this volume)

37.3 RESULTS

To investigate internal feedbacks triggered by changes in insolation, atmospheric climatologies are averaged between 127 000–125 000 yr BP and 116 000–114 000 yr BP. These time intervals roughly correspond to the maximum and minimum extremes in the temperature response along the transient simulations. The difference in climatology between the two time slices (115 000–126 000 yr BP) therefore reflects the total response to insolation in the transient experiments. Accordingly, the following results are being interpreted as warming/cooling anomalies with reference to the 115 000 yr BP climate.

Figure 37.2 displays the 2-m temperature difference between 115 000 and 126 000 yr BP. In both experiments, a strong cooling is simulated in the northern hemisphere which is more intense over continents than over oceans. The cooling over the ocean is strongest in the North Pacific with anomalies of more than 4 K in the western area. The weaker cooling in the North Atlantic is related to convective deep mixing in this area which transports warm surface waters to depth. In external forced warming (cooling) scenarios, this will decrease (increase) the net oceanic heat loss to the atmosphere. Accordingly, this convective damping leads to lower cooling anomalies in the North Atlantic compared to the North Pacific.

Strongest cooling is observed over the Arctic area where the increase in sea-ice thickness (not shown) amplifies the cooling. Additionally the advance in sea-ice extent at 115 000 yr BP leads to thermal insulation of the ocean and thus decreases the oceanic heat loss to the atmosphere.

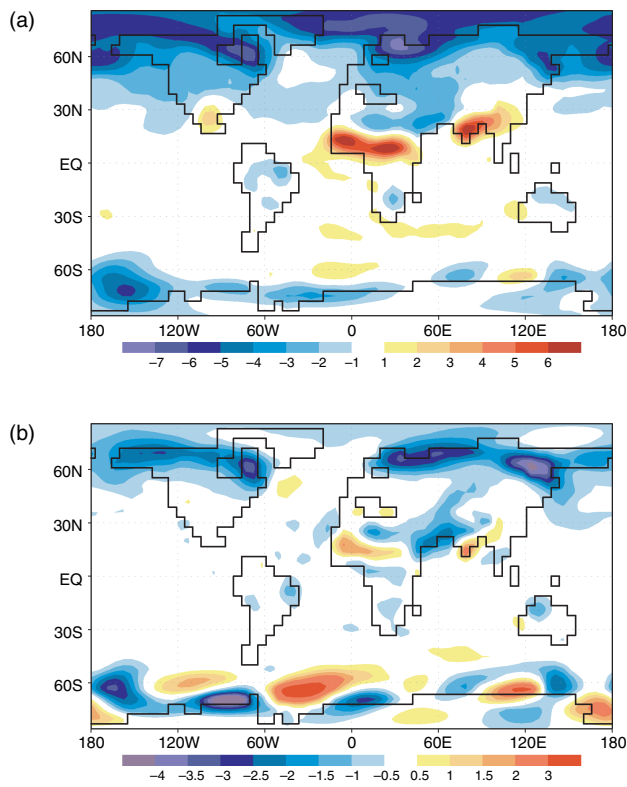


Fig. 37.2 (a) Yearly mean 2-m temperature difference between 126 and 115 kyr BP displayed for the experiment with feedback. (b) Difference between (a) and experiment without feedback.

Differences between the two Eemian experiments are predominantly found in boreal regions (Fig. 37.2b). In these regions, the temperature response is already large in the model with prescribed vegetation. This is the direct effect of expanded snow covered areas that translates into a higher surface albedo (not shown), leading to reduced absorption of short-wave radiation.

In the fully coupled model, however, cooling anomalies exceed 4 K over wide areas in the northeast of Siberia and Alaska and even 6 K over eastern Canada and Scandinavia. The underlying principle for these strong local cooling patterns is the replacement of boreal forests by tundra during the late Eemian. The resulting decrease in vegetation cover has an additional impact on the surface albedo.

Figure 37.3 illustrates the yearly cycles of land surface albedo averaged between 60 and 90°N for 126 and 115 000 yr BP. The

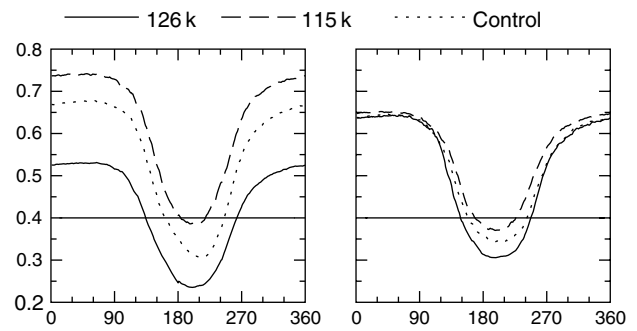


Fig. 37.3 Seasonal cycle of simulated land surface albedo north of 60°N. Left (right) panel shows experiment with (without) feedback.

vegetation feedback is seen throughout the whole year but becomes largest during winter. This is because the influence of snow on surface albedo is weaker in forest-covered areas compared to grasslands that predominates the fixed ECHAM3 vegetation over most of the boreal regions. At 126 000 yr BP, the maximum winter (summer) land albedo of the model with nondynamic vegetation exceeds that of the fully coupled model by ~ 0.11 (~ 0.07). This corresponds to a relative increase of about 21% in winter and 29% in summer. The replacement of boreal forest by tundra at 115 000 yr BP has the consequence that the maximum winter (summer) albedo of the fully coupled model exceeds that of the model with nondynamic vegetation by ~ 0.09 (~ 0.02) which corresponds to a lowering of 12% (5%). This vegetation-related albedo effect enhances (lowers) the temperatures at 126 000 yr BP (115 000 yr BP) in the experiment with included feedback which explains the stronger response seen in temperature (Fig. 37.2).

Besides this, also the seasonal length with very low summer land albedo below 0.4 varies with the choice of the coupling setup. At 115 000 yr BP, this season is 24 days shorter in the simulation using interactive vegetation whereas at 126 000 yr BP it is 30 days longer.

In agreement with the forcing (Fig. 37.1a), the southern hemisphere experiences slight warming (< 1 K) at 115 000 yr BP. Only in the subtropics, a weak cooling is simulated

due to a higher cloud cover and increased evaporative cooling. This is a consequence of an overall strengthening of the southern hemisphere monsoon system.

Strong warming anomalies seen in the northern African tropics, over India, and Mexico (Fig. 37.2a) indicate a negative feedback simulated in both experiments. In these regions, a lower cloud cover during northern hemisphere summer decreases the surface radiation. Here, the largest reductions in precipitation are found, which also decreases evaporative cooling (Fig. 37.4a). Precipitation anomalies exceed 25 mm/month in Mexico, 75 mm/month in northwest Africa and 100 mm/month in southeast India in the experiment with interactive vegetation. These changes reflect a weakened monsoon as a consequence of lower land–sea temperature contrasts during the late Eemian. Again, the changes in precipitation are weaker when applying fixed vegetation (Fig. 37.4b). The difference is extreme in the Sahara desert where precipitation decreases during the monsoon season by about 170 mm/month in the full model, whereas with prescribed vegetation it is decreased by only 72 mm/month. This difference refers to a strong albedo feedback due to the vanishing vegetation in this region. Over wide areas, the darker temperate grasslands are replaced by lighter desert surfaces which increase the local surface albedo by up to 0.10. As a result, the area that benefits from monsoon precipitation is restricted to the south (Fig. 37.4).

The time-transient evolution of yearly mean precipitation averaged over the Sahara desert (10°W – 20°E ; 10° – 30°N) is shown in Fig. 37.5. A maximum is reached between 126 000 and 125 000 yr BP in both model versions, but the changes simulated by the fully coupled model are more than twice as strong. In the experiment without feedback, a monotonous decrease follows indicating a more or less linear response to the forcing. By contrast, when the vegetation feedback is included, a rapid transition to drier conditions is seen between 125 500

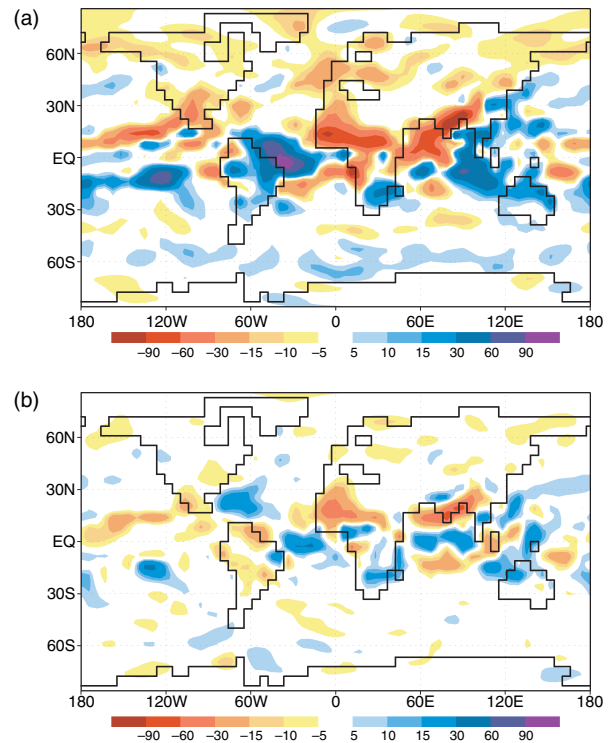


Fig. 37.4 (a) Yearly mean precipitation difference between 126 and 115 kyr BP displayed for the experiment with feedback. (b) Difference between (a) and the experiment without feedback.

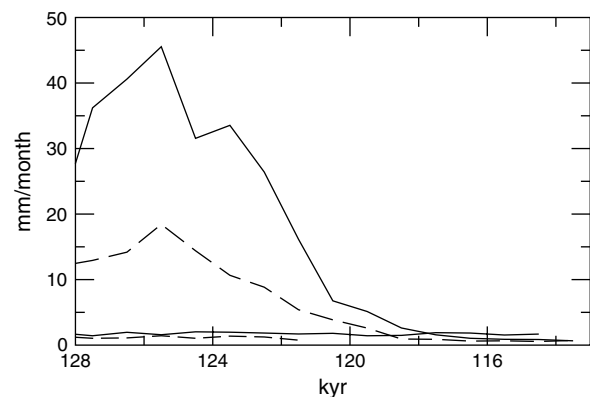


Fig. 37.5 Time series of annual mean precipitation over the Sahara Desert [10°W – 20°E ; 10° – 30°N]. Displayed are 1000-year averages. Dashed lines indicate the experiments with prescribed vegetation. Thin lines indicate the control experiments.

and 124 500 yr BP and from 123 500 to 120 500 yr BP followed by a slight decreasing trend. The steep decreases in precipitation are accompanied (with a little phase lag) by drastic reductions in vegetation

cover (not shown) which then accelerate the transition to drier conditions. From about 118 000 yr BP, the two curves are virtually indistinguishable from the two control experiments.

Higher precipitation is seen in South America, South Africa and over Australia (Fig. 37.4a) which is consistent with the intensified southern hemisphere monsoon. An extraordinary increase is observed over the tropical western Atlantic, resulting from a stronger atmospheric convergence in this area as indicated in the velocity potential fields (not shown) during boreal summer.

37.3.1 Changes in vegetation

The changes in temperature and precipitation have a large impact on the terrestrial biosphere. The most prominent changes are seen in regions with strong climatic feedback. The entire boreal belt suffers under the strong cooling in the high northern latitudes and shows reductions in vegetation cover larger than 75%. These changes monitor mainly the southward retreat of boreal forests which (in the vicinity of the North Atlantic warm anomaly and a more northern position of the westerlies at 126 000 yr BP) formerly reached the Arctic Ocean in northern Europe and northwestern Asia (Fig. 37.6a).

Changes of similar magnitude are found in the African tropics and south-east Asia. In Africa, the tropical forests and adjacent savanna retreat southward and temperate grasslands vanish in the western part of the Sahara desert. In South-east Asia, tropical forests retreat to the south and completely disappear in India (Fig. 37.6).

In semiarid regions between 30 and 50°N that are not affected by changes in the monsoon system vegetation, cover is slightly increased. This refers mainly to the appearance of forests. These continental regions are characterized by strong cooling anomalies especially during the growing season but only moderate decreases in rainfall (<5 mm/month over most of these areas).

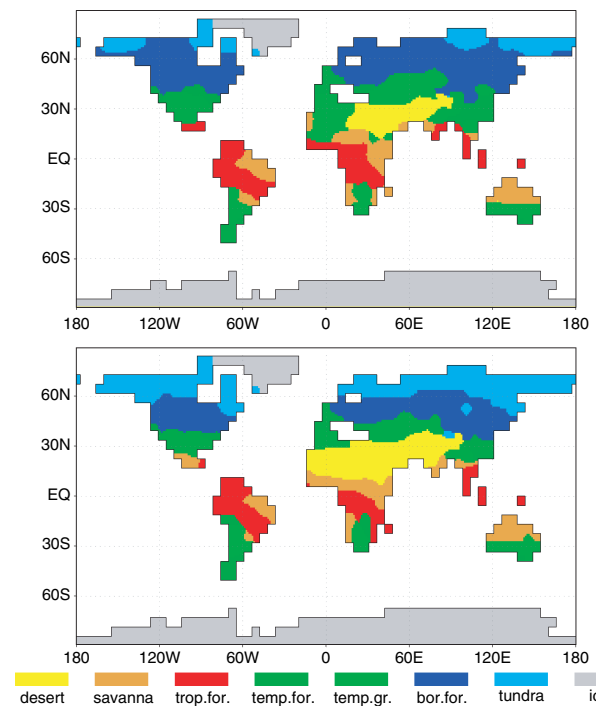


Fig. 37.6 Simulated ecosystem distribution for (a) 126 kyr BP and (b) 115 kyr BP.

Such conditions decrease the stress for water-demanding PFT, thus favouring rather humid ecosystems. Slight increases in vegetation cover are found also in the southern continents in areas that benefit from intensified monsoon precipitation (Fig. 37.4).

The changes in the terrestrial biosphere and climate have only minor consequences for the terrestrial carbon storage which varies by only ~ 107 GtC (Fig. 37.7) along the last interglacial. In case of the vegetation (litter) stock, an upper limit is reached in the course of the Eemian at roughly 1050 (640) GtC which is reduced by more than 10% ($\sim 15\%$) at the end of the experiment. Intensified decomposition dominates the soil carbon in the early warmer part of the Eemian which reduces this stock and counteracts the increase in vegetation and litter. The total carbon storage which reflects the net effect of all processes thus reaches its maximum when the climate has cooled down moderately to improve soil carbon preservation but is still warm enough to maintain boreal forests in the high latitudes.

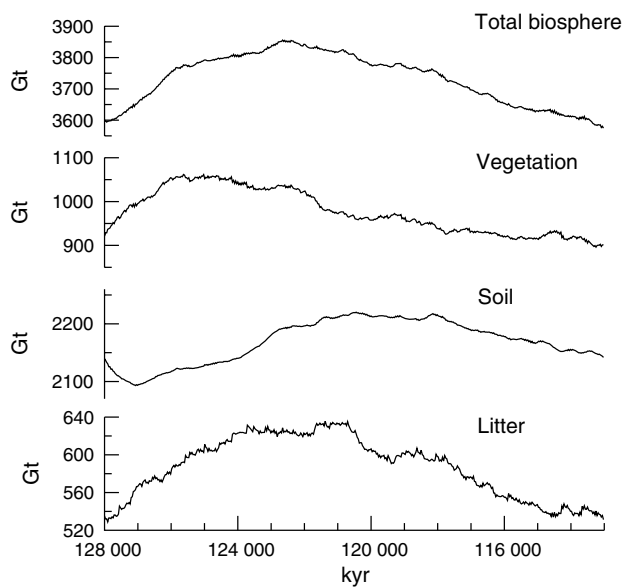


Fig. 37.7 Time series of carbon storage for the experiment with vegetation feedback.

37.4 TIME-TRANSIENT SENSITIVITY OF TEMPERATURE TO CHANGES IN INSOLATION

Figure 37.1d shows the temperature response averaged over landpoints between 60 and 90°N for the two experiments in increments of thousand-year averages. In the experiment with interactive vegetation, the near-surface temperature falls by 4.8 K from its Eemian maximum to -19.5°C at the end of the experiment. In the experiment with fixed vegetation, the decrease is only 3.0 K. This corresponds to $\sim 60\%$ of the 4.8 K decrease in the fully coupled model, while the two control experiments are statistically indistinguishable. The higher sensitivity of the fully coupled model mainly reflects the dynamic changes in vegetation cover and associated albedo changes described above. The difference between the two model versions fades towards 121 500 yr BP when the insolation becomes similar to that of the control run. They are virtually indistinguishable up to $\sim 117 500$ yr BP which is relatively long considering the steeply decreasing insolation at that time (Fig. 37.1a). This reflects the fact that the

prescribed ECHAM3 vegetation has already an overall lower vegetation cover in boreal regions compared to the control run of the fully model. Because of the same reason, the difference between the two curves is slightly lower at the end of the experiments than during the Eemian, but nevertheless it is significant. The standard deviation of differences between the two control experiments shown in Fig. 37.1d (thin lines) is 0.26 K, while the maximum difference between the Eemian experiments amounts to 0.96 K at 113 500 yr BP which is more than the three-fold standard deviation.

The time-transient evolution of sea-surface temperatures in the North Atlantic shows a significant amplification of the warming when using the fully coupled model (Fig. 37.1b). This is related to stronger atmospheric warming over land (Fig. 37.1d) which translates into the ocean mainly via the ocean–atmosphere heat fluxes. In case of the North Atlantic, the heat loss to the atmosphere is up to 0.1 PW lower in the experiment with dynamic vegetation during the maximum warming period.

Another effect is seen in the shape of the following cooling period in the North Atlantic. When using prescribed vegetation, cooling starts at $\sim 125 500$ yr BP proceeding to the end of the experiment indicating a nearly linear response to the forcing. In the fully coupled model, the beginning of the cooling period is clearly delayed. Again, the delay is linked to the evolution over land where anomalous high temperatures (compared to the model without feedback) prevail until 122 500 yr BP and go against the astronomical cooling signal. After 122 500 yr BP, vegetation is progressively diminished (1c) and the cooling accelerates over land.

37.5 DISCUSSION AND CONCLUSIONS

The results demonstrate a substantial amplification of insolation-forced climate feedbacks when using interactive dynamical

vegetation instead of nondynamic prescribed vegetation.

The overall rationale behind these feedbacks is changes in surface albedo due to land surface dynamics that further affect temperature and precipitation. Two main feedbacks that are amplified by vegetation dynamics have been demonstrated:

- 1) boreal vegetation–temperature feedback, and
- 2) low-latitude vegetation–monsoon feedback

The simulated climate and vegetation pattern agree with results from other model studies (an overview can be found in Kabat *et al.*, 2003) and are well supported by palaeoclimatic reconstructions. Pollen spectra and macrofossil assemblages from the Noatak Basin indicate extended distribution of boreal forests in Alaska during the last interglacial (Muhs *et al.*, 2001; Edwards *et al.*, 2003). Similar changes are preserved in deposits from the St Lawrence estuary in Quebec where a shift from boreal forests to tundra vegetation at the end of the last interglacial is recorded by pollen spectra (Clet and Occhietti, 1995).

Likewise, the simulated intensification of the northern hemisphere monsoon system is in excellent agreement with proxy data. In particular, the greening of the western part of the Sahara desert during the Eemian is supported by reconstructions from pollen records (van Andel and Tzedakis, 1996). Jahns *et al.* (1998) provided evidence for drier conditions during glacial periods compared to interglacials in the African tropics.

Jiang and Ding (2005) recently presented pollen records from the South China Sea that indicate humid climatic conditions to be more abundant in the area of the Chinese Loess Plateau in interglacial and interstadial periods during the last 130 kyr. Furthermore, the distribution of deserts and sandy land in China was greatly reduced during the last interglacial period, and the mobile dune area was about two-thirds of that of

today (Chen *et al.*, 2004). Moreover, lighter interglacial planktonic $\delta^{18}\text{O}$ values found in long-term records from core locations in the South China Sea point to a generally stronger East Asian summer monsoon during the Quaternary warm periods (Jun *et al.*, 2004).

In contrast, the simulated weaker Northern Australia monsoon seems to be in conflict with palaeoenvironmental data reported in Veeh *et al.* (2000), indicating generally wetter conditions in this region during interglacials.

The northern hemisphere temperatures over land and even in the uppermost ocean layer showed a more linear response to insolation forcing when using prescribed vegetation instead of dynamic vegetation. With regard to the last glacial inception, the boreal temperature feedback at 115 000 yr BP together with changes in sea ice cover appears to be an essential precondition for the inception of continental ice sheet growth.

REFERENCES

- Arakawa, A., and Lamb, V.R., 1977. Computational design of the basic dynamical processes of the UCLA general circulation model. *Methods Comput. Phys.* 16, 173–283.
- Berger, A., and Loutre, M.F., 1991. Insolation values for the climate of the last 10 million years. *Quat. Sci. Rev.* 10, 297–317.
- Chen, H.Z., Su, Z.Z., Yang, P., and Dong, G.R. 2004. Preliminary reconstruction of the desert and sandy land distributions in China since the last interglacial period. *Science in China Series D-Earth Sciences* 47, 89–100.
- Claussen, M., and Gayler, V., 1997. The greening of the Sahara during the mid-Holocene: Results of an interactive atmosphere-biome model, *Global Ecology and Biogeography Letters* V6(N5), 369–377.
- Claussen, M., Brovkin, V., Petoukhov, V., and Ganopolski, A., 2001. Biogeophysical versus biogeochemical feedbacks of large-scale land-cover change. *Geophys. Rev. Letters* 26(6), 1011–1014.
- Clet, M., and Occhietti, S., 1995. Pollen content of Sangamonian interglacial deposits, Ile-aux-Coudres, Middle St-Lawrence-estuary, Quebec. *Géographie Physique et Quaternaire* 49(2), 291–304.

- Crucifix, M., and Loutre, M.F., 2002. Transient simulation over the last interglacial period (126–115kyr BP): feedback and forcing analysis. *Clim. Dyn.* 19, 417–433.
- Edwards, M.E., Hamilton, T.D., Elias, S.A., Bigelow, N.H., and Krumhardt, A.P., 2003. Interglacial extension of the boreal forest limit in the Noatak Valley, northwest Alaska: Evidence from an exhumed river-cut bluff and debris apron. *Arctic Antarctic and Alpine Research* 35(4), 460–468.
- Harrison, S.P., Kutzbach, J.E., Prentice, I.C., Behling, P.J., and Sykes, M.T., 1995. The response of northern hemisphere extratropical climate and vegetation to orbitally induced changes in insolation during the last interglaciation. *Quat. Res.* 43, 174–184.
- Jahns, S., Huls, M., and Sarnthein, M., 1998. Vegetation and climate history of west equatorial Africa based on marine pollen record off Liberia (site GIK 16776) covering the last 400,000 years. *Rev. Paleobot. Palynol.* 102, 277–288.
- Jiang, H., and Ding, Z., 2005. Temporal and spatial changes of vegetation cover on the Chinese Loess Plateau through the last glacial cycle: evidence from spore-pollen records. *Review of Palaeobotany and Palynology* 133, 23–37.
- Jun, T., Wang, P.X., and Cheng, X.R., 2004. Development of the East Asian monsoon and Northern Hemisphere glaciation: oxygen isotope records from the South China Sea. *Quat. Sci. Rev.* 23(18–19), 2007–2016.
- Kabat, P., Claussen, M., Dirmeyer, P.A., Gash, J.H.C., Bravo de Guenni, L., Meybeck, M., Pielke, R.S., Vörösmarty, C.J., Hutjes, R.W.A., Lütke-meier, S. (Eds.), 2003. *Vegetation, Water, Humans and the Climate: A New Perspective on an Interactive System*. Global Change – The IGBP Series, 566 pp, Springer Verlag, Berlin, Heidelberg.
- Kubatzki, C., Montoya, M., Rahmstorf, S., Ganopolski, A., and Claussen, M., 2000. Comparison of the last interglacial climate simulated by a coupled global model of intermediate complexity and an AOGCM. *Clim. Dyn.* 16, 799–814.
- Larrasoana, J.C., Roberts, A.P., Rohling, E.J., Winkhofer, M., and Wehausen, R., 2003. Three million years of monsoon variability over the northern Sahara. *Clim. Dyn.* 21(7–8), 689–698.
- Levis, S., Bonan, G.B., and Bonfils, C., 2004. Soil feedback drives the mid-Holocene North African monsoon northward in fully coupled CCSM2 simulations with a dynamic vegetation model. *Clim. Dyn.* 23, 791–802.
- Maier-Reimer, E., Mikolajewicz, U., and Hasselmann, K., 1993. Mean circulation of the Hamburg LSG OGCM and its sensitivity to the thermohaline surface forcing. *Journal of Physical Oceanography* 23, 731–757.
- Meissner, K.J., and Gerdes, R., 2002. Coupled climate modelling of ocean circulation changes during ice age inception. *Clim. Dyn.* 18, 455–473.
- Meissner, K.J., Weaver, A.J., Matthews, H.D., and Cox, P.M., 2003. The role of land surface dynamics in glacial inception: a study with the UVic Earth system model. *Clim. Dyn.* 21, 515–537.
- Montoya, M., Crowley, T.J., and von Storch, H., 1998. Temperatures at the last interglacial simulated by a coupled ocean–atmosphere climate model. *Paleoceanography* 13(2), 170–177.
- Montoya, M., Crowley, T.J., and von Storch, H., 2000. Climate simulation for 125 kyr BP with a coupled ocean–atmosphere general circulation model. *J. Clim.* 13, 1057–1072.
- Muhs, D.R., Ager, T.A., and Beget, J.E., 2001. Vegetation and paleoclimate of the last interglacial period, central Alaska. *Quat. Sci. Rev.* 20(1–3), 41–61.
- Roeckner, E., Arpe, K., Bengtsson, L., Brinkop, S., Dömenil, L., Esch, M., Kirk, E., Lunkeit, F., Poneter, M., Rockel, B., Sausen, R., Schlese, U., Schubert, S., and Windelbrand, M., 1992. Simulation of present day climate with the ECHAM model: impact of the model physics and resolution. Max Planck Institute for Meteorology, Hamburg, Rep. 93.
- Sitch, S., Smith, B., Prentice, I.C., Arneth, A., Bondeau, A., Cramer, W., Kaplan, J., Levis, S., Lucht, W., Sykes, M., Thonicke, K. and Venevski, S., 2003. Evaluation of ecosystem dynamics, plant geography and terrestrial carbon cycling in the LPJ dynamic vegetation model. *Global Change Biology* 9, 161–185.
- van Andel, T.H., and Tzedakis, P.C., 1996. Paleolithic landscapes of Europe and environments: 150 000–25 000 years ago: an overview. *Quaternary Sci. Rev.* 15, 481–500.
- Voss, R., and Sausen, R., 1996. Techniques for asynchronous and periodically synchronous coupling of atmosphere and ocean models Part II impact of variability. *Clim. Dyn.* 12, 605–614.
- Veeh, H.H., McCorcle, D.C., and Heggie, D.T., 2000. Glacial/interglacial variations of sedimentation on the West Australian continental margin: constraints from excess ^{230}Th . *Marine Geology* 166, 11–30.
- Yoshimori, M., Reader, M.C., Weaver, A.J., and McFarlane, N. A., 2002. On the causes of glacial inception at 116 kaBP. *Clim. Dyn.* 18, 383–402.
- Yuan, D.X., Cheng, H., Edwards, R.L., Dykoski, C.A., Kelly, M.J., Zhang, M.L., Qing, J.M., Lin, Y.S., Wang, Y.J., Wu, J.Y., Dorale, J.A., and An, Z.S., Cai, Y.J., 2004. Timing, duration, and transitions of the last interglacial Asian monsoon science 304, 575–578.